Space Vector PWM Control Synthesis for a H-Bridge Drive in Electric Vehicles

Kolli Abdelfatah, Olivier Béthoux, Alexandre de Bernardinis, Eric Labouré, Gérard Coquery

Space Vector PWM Control Synthesis for a H-Bridge Drive in Electric Vehicles

A. Kolli[1], *Student Member, IEEE,* O. Béthoux[2], *Member, IEEE,* A. De Bernardinis[1], *Member, IEEE,* E. Labouré[2], and G. Coquery[1].
olivier.bethoux@lgep.supelec.fr
alexandre.de-bernardinis@ifsttar.fr

***Abstract*—This paper deals with a synthesis of Space Vector PWM control methods applied for a H-bridge inverter feeding a 3-phase Permanent Magnet Synchronous Machine in Electric Vehicle application. First, a short survey of existing power converter architectures, especially those adapted to degraded operating modes, is presented. Standard SVPWM control methods are compared with three innovative ones using EV-drive specifications in the normal operating mode. Then, a rigorous analysis of the margins left in the control strategy is presented for a semiconductor switch failure to fulfill degraded operating modes. Finally, both classic and innovative strategies are implemented in numerical simulation; their results are analyzed and discussed.**

***Index Terms*—Motor drives, Inverters, Space vector pulse width modulation (SVPWM), Permanent magnet machines, Semiconductor device reliability**

I. INTRODUCTION

Power converters are increasingly used in automotive applications for many reasons such as power conditioning, power management, and consumption reduction. As for any embedded transportation system, these power converters are subject to severe constraints especially regarding compactness and vehicle integration. More specifically electric vehicles (EVs) require a high degree of availability (continuity of service). In particular the constraining automotive environment is characterized by severe traction-braking cycles which induce power and thermal cycling during running phases of the vehicle [1]–[2]. Indeed, thermo-mechanical stresses have a significant impact on the lifetime power switches [3]. Consequently, there is a degradation of the semiconductor devices, which finally forces them into a failed state: short-circuit (SC) or open-circuit (OC) [2]. Such failures occurring on single power switches can affect the function of power converters and spread through the traction chain elements. It is then necessary to first isolate the fault, confine it and lastly reconfigure the control algorithms to operate in the presence of the fault. Obviously, the topology of the power converters or the power chain must be adapted to allow operation in degraded mode:

– by associating a fourth additional half bridge in a three-phase inverter topology connected to the neutral point of the electric motor [4].

1 IFSTTAR/COSYS/LTN-*Laboratoire des Technologies Nouvelles*
2 LGEP-*Laboratoire de Génie Electrique de Paris*

– by using multilevel inverters topologies used in a high power traction drive [5].

– by redistributing the control efforts in a four-wheel independently driven electric vehicles [6]…

Furthermore, faults may also happen on sensors and can be taken into account by active fault-tolerant control systems. For example in [7]–[8], authors consider a high-performance induction-motor drive for an EV or a hybrid one (HEV). The proposed systems detect a sensor loss or a sensor recovery and dynamically change its strategies to sustain the best control performances.

Besides, faults may also occur in the electrical machine and can be considered using fault-tolerant designs, as example for a redundant IPM (Interior Permanent Magnet) motors structure [9].

In this paper, a specific fault-tolerant drive topology patented by Valeo Company [10]–[11] is studied. It allows both traction and charger operating modes with the same power electronics devices [12]–[13]. Furthermore, the traction operating mode is fault-tolerant as it can operate with only two phases of the electrical machine.

The considered topology uses six half bridges instead of a three classical one, leading to a much higher complexity of the control strategies but offering new voltage configurations. So, these degrees of freedom are used to design new control methods and will be compared with classical ones in this paper. The next issue is to investigate whether the innovative control methods can be reconfigured in a switch failure case. Both presentations are based on space vector pulse width modulation technique (SVPWM), which allows the proper analysis of this discrete control problem and to synthesize suitable control strategies.

The paper is organized as follows: Section II deals with power electronic architecture tolerant to semiconductor failure in EV drive. Section III discusses modeling and control drive requirements. Section IV focuses on SVPWM control synthesis for normal operating mode. Comprehensive analysis of the failure is conducted in section V. Finally, the section VI draws conclusions and perspectives.

II. Power Electronic Architecture Tolerant To Semiconductor Failure In EV Drive

Semiconductors are an important source of failure in traction systems. Investigations have highlighted the failure rate per element in a traction system [14]. Authors assess that the semiconductor failures and their driver auxiliary circuit are the most recurrent in electric automotive

applications. Using reliability prediction methods, authors in [14] point out that there is a reasonably equal repartition between faults occurring in the semiconductors and their auxiliary circuits. They estimate that about 40% of failures can be attributed to semiconductors faults and 39□ to their auxiliary circuits. Driver circuits should be reliable enough, to prevent additional sources of failure [15].

Automotive is a constraining environment: start-stop cycles, power and thermal cycles, confined areas with thermal constraints [16]. In this severe environment, power semiconductors are the most sensitive elements in terms of lifetime and reliability. They are subject to electro-thermal and also mechanical stresses, accelerating their failure mechanisms [17]. These failures are mainly induced by power and thermal cycling of the semiconductor device [18]. For example, an interesting investigation conducted on a Renault Kangoo electric vehicle has been carried out in [19]. The authors have demonstrated that direct silicon temperature measurement of an operating traction inverter is feasible. As a result, authors establish an accurate thermal model of the IGBT traction inverter which can be applied in real-time EV application. Several papers have also been published on the topic of power modules accelerated ageing tests (thermal cycling and power cycling) in order to estimate the level of semiconductors expectancy lifetime [17]–[18] and to study the failure mechanisms and effects [18]–[20]–[21]. It has been reported that repetitive failures have two different sources: an external one which can be, for example, linked to faulty control signal [22] and an internal one, linked to physical degradation of the power semiconductor. Examples of these internal failures are: bond wire lift off, gate leakage failure and damages on semiconductors chip and solder [18], SiAl contact ageing [21], electro-migration effect [20], latch-up [23]. These internal failures can modify the operating state of the semiconductor and induce abnormal behavior like OC or SC states. These power switch malfunctions decrease the number of discrete voltages that the voltage inverter can apply to the machine. Consequently this new limitation prevents a suitable magnetic field rotation in the rated torque and speed frame. Moreover the rated control algorithm imposes voltages that are not necessarily applied to the motor. In conclusion these abnormal states affect the power converter function, which impacts the motor operating behavior and consequently the traction powertrain,

compromising the vehicle driver safety. Indeed, a switch failure in standard 3-leg inverter influences drastically the motor behavior and prevents continuity of service [24].

Current technology provides “smart” drivers that can provide early detection of a fault occurring in the power switch and return a feedback fault signal. For instance cross conduction is usually handled by a soft turn-off once a fast desaturation detector raises the alarm. This information should be exploited by the control strategy interface in the objective of diagnostic, protection (fault confining) and reconfiguration

to an adequate strategy.

In case of failure affecting a machine phase, a particular remedial strategy has been reported in [4]. After fault isolation which inhibits one motor phase, authors propose to connect the motor star point to an additional fourth leg. This choice is performed in order to allow the flow of the neutral current, while the other two motor phases remain supplied. Fig. 1 presents this fault tolerant architecture. However, the proposed solution requires the use of contactors for fault isolation; this is a drawback in electric vehicle applications, in particular regarding cost and reliability of such solutions. Welchko et al. listed many interesting fault-tolerant AC motor drive topologies that unfortunately face the same drawback [25]. This paper investigates another solution, which offers a greater ability for reconfiguration. The power structure is composed of 3 H-bridges, each of them supplying a separate PMSM motor phase. The proposed architecture does not require the fault-isolation contactors. As shown in Fig. 2, the 3H-Bridge converter uses a machine without neutral point. The advantage of this architecture is to allow the application of the full DC link voltage to each PMSM stator winding [10]–[12]–[26]. However, with this specific architecture, the zero-sequence current is not structurally rejected, unlike the classical solution with a star neutral point topology [27]. The control of the converter should fulfill two requirements: optimal working in normal mode, and in degraded mode. Obviously the proposed 3 H-bridge architecture based on 12 switches involves a higher number of semiconductor devices, but offers many redundancy possibilities in degraded mode using only two bridges. Two points may be noted:

–A competing configuration using the same number of power switches (12) is reported in [28]–[29]. This paper proposes a four-level voltage source inverter topology (dual-inverter) but uses two isolated

and unequal dc-link voltages. Other authors suggest segmenting the power source with two converters feeding double-star synchronous machines. This architecture is fault-tolerant and ensures minimum loss control under fault phase conditions [30]–[31].

–A major advantage of our structure is, besides the operation in traction mode, the ability to operate in battery recharge mode with the same hardware, namely the power converter and the electric machine. This is achieved through the PM machine windings, which has a phase middle point for direct connection to the recharging network (Fig. 2). In this mode, the motor phases used as a filter inductances are subdivided in two half windings. The middle point is used to inject currents [12]–[13].

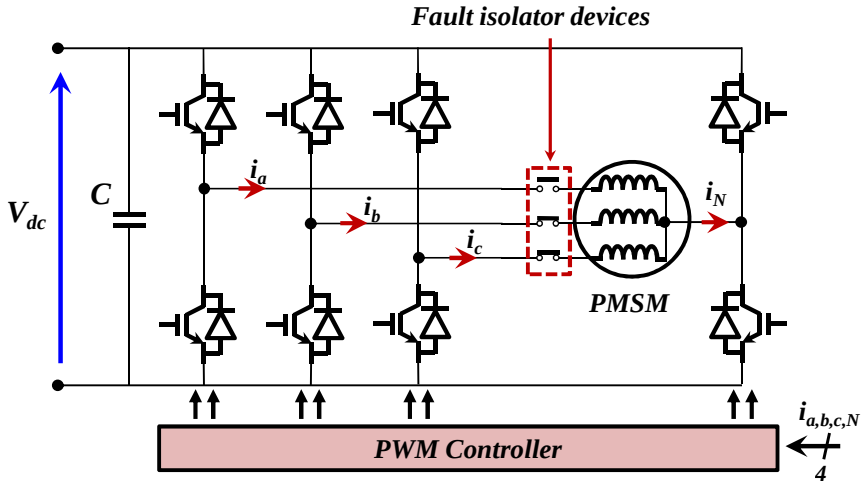

Fig. 1. Fault-tolerant scheme of 4-leg inverter drive [4].

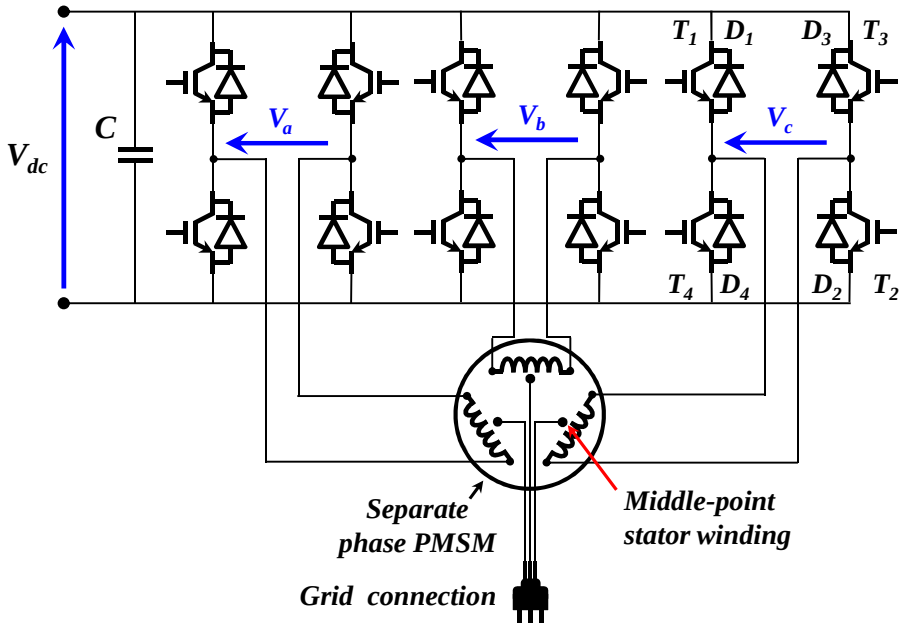

Fig. 2. Studied architecture: PMSM drive fed by 3 H-Bridge inverters.

III. Modeling And Control Drive Requirements

The set of the PMSM and its 3-H bridge inverter is first described in a control model approach (III-A and III-B). Secondly, this model highlights the key issues that the control algorithm must satisfy (III-C). Next, the listed requirements allow the discussion of the innovative PWM control method and to classify classic and new strategies (III-D to III-F). Finally the chosen method is implemented in a MATLAB/Simulink software platform (III-G).

A. Drive Control Modeling In Concordia reference frame

The studied motor is a non-saturated non-salient pole permanent magnet synchronous machine and no damping effect is considered. The three-stator winding is constructed to give a sinusoidal air-gap flux distribution; similarly, specially shaped rotor magnets provide sinusoidal flux within the air gap. The Concordia transform (CT) has proved to simplify motor drive control [32]. Using the generalized power invariant CT enables to diagonalize the stator inductance matrix.

$$\begin{cases} V_0 = R \cdot i_0 + L_0 \dfrac{d}{dt} i_0 + e_0 \\ \begin{bmatrix} V_\alpha \\ V_\beta \end{bmatrix} = R \cdot \begin{bmatrix} i_\alpha \\ i_\beta \end{bmatrix} + \begin{bmatrix} L_c & 0 \\ 0 & L_c \end{bmatrix} \dfrac{d}{dt} \begin{bmatrix} i_\alpha \\ i_\beta \end{bmatrix} + \begin{bmatrix} e_\alpha \\ e_\beta \end{bmatrix} \end{cases} \quad (1)$$

Because the motor phases are not electrically connected one to the other, the sum of the three phase currents is not constrained. Thus, for the proposed motor drive architecture, zero-sequence current is not forced to be null and (1) reveals two fictitious machines associated to 2 orthogonal eigenspaces related to the 0-line and the α-β frame [33]–[34]–[35].

1. First, the *Zero-sequence fictitious machine* is associated to the leakage inductance L_0 and back EMF e_0 component induced by the rotor rotation. Assuming perfectly balanced back electromotive forces in the three windings, e_0 is null. Therefore, this fictitious machine does not produce any electromagnetic torque. However, its current i_0 creates unnecessary ohmic losses.

2. Second, the *main fictitious machine* is associated to the cyclic inductance L_c and the back EMF $e_{\alpha\beta}$ components. Thus, the instantaneous electromagnetic torque is given by:

$$T_{em} = \frac{1}{\Omega}\left(e_\alpha \cdot i_\alpha + e_\beta \cdot i_\beta\right) \quad (2)$$

Where Ω is the motor speed. The main motor drive objectives are to produce a desired torque while minimizing the Joule losses [36]. These goals are achieved by controlling the inverter power switches. The next subsection explains the dedicated 3H-Bridge converter potentials.

B. Space Vector PWM Control Approach

As presented in Fig. 2, the stator winding terminals are directly connected to one H-bridge. Each H-bridge has four discrete states but can only produce three discrete voltage levels, namely $+V_{dc}$, 0 and $-V_{dc}$. Together the 3-phase H-Bridge inverter provides 27 switching states. To match the PMSM multimachine representation, the output voltage vectors are described in the Concordia reference frame (Fig. 3). The stator voltages are divided into four main families [37] according to magnitude and zero-sequence component values. These families are summarized in the following Table I:

TABLE I
STATOR VOLTAGES FAMILY DECOMPOSITION

FAMILIES	VOLTAGE VECTORS	MAGNITUDE	V_0 VALUE
Family I	15, 17, 18, 23, 24, 26	$V_{dc} \cdot 2\sqrt{2/3}$	$\pm V_{dc} \cdot \sqrt{1/3}$
Family II	6, 8, 12, 16, 20, 22	$V_{dc} \cdot \sqrt{2}$	0
Family III	2, 3, 4, 7, 10, 19	$V_{dc}\sqrt{2/3}$	$\pm V_{dc} \cdot \sqrt{1/3}$
Family IV	5, 9, 11, 13, 21, 25	$V_{dc}\sqrt{2/3}$	$\pm V_{dc} \cdot 2\sqrt{1/3}$
Family V	1	0	0
Family VI	14, 27	0	$\pm V_{dc} \cdot \sqrt{3}$

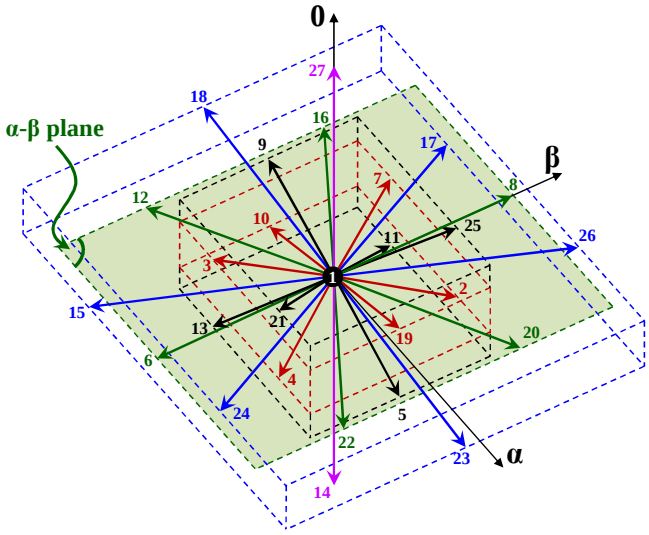

Fig. 3. 3H-Bridge inverter switching states and space vectors.

To control both fictitious machines, the PMSM controller requires a particular space vector $[V_0^* \; V_\alpha^* \; V_\beta^*]^T$. The 3-H bridge inverter can only provide an average value of this voltage setpoint, using pulse-width modulation (PWM) technique. PWM also produces voltage harmonics that can be controlled by monitoring switching frequency. Consequently, the PWM generation is a 4-dimensional problem: Two dimensions are devoted to the main machine, one dimension is linked to the zero-sequence machine and the last one permits to meet the time constraint. Therefore 4 different discrete voltage vectors $\{V_1, V_2, V_3, V_4\}$ among the 27 inverter possibilities are necessary for solving this Space Vector PWM problem [38]–[39]. Noting T_{sw} the desired switching period, the 4 associated durations $\{\Delta t_1, \Delta t_2, \Delta t_3, \Delta t_4\}$ are computed using (3):

$$\begin{bmatrix} V_0^* \\ V_\alpha^* \\ V_\beta^* \\ 1/2 \end{bmatrix} = \frac{1}{T_{sw}} \begin{bmatrix} V_{01} & V_{02} & V_{03} & V_{04} \\ V_{\alpha 1} & V_{\alpha 2} & V_{\alpha 3} & V_{\alpha 4} \\ V_{\beta 1} & V_{\beta 2} & V_{\beta 3} & V_{\beta 4} \\ 1 & 1 & 1 & 1 \end{bmatrix} \begin{bmatrix} \Delta t_1 \\ \Delta t_2 \\ \Delta t_3 \\ \Delta t_4 \end{bmatrix} \qquad (3)$$

The set of four voltage vectors is chosen to guarantee that each Δt_k is positive. In 3-H bridge case there are numerous ways of choosing such a set. The main issue of this section is to select the most relevant one. The next sub-section clarifies the PMSM SVPWM specifications.

C. Control Drive Requirements

The SVPWM has to control the 3-H bridge inverter in order to maximize the drive performances and minimize the global power losses.

The first objective is to optimize the electromechanical functioning in the torque - speed frame [40]. At high speed, the ohmic losses can be neglected ($L_c\omega >> R$) and the base speed Ω_b can be expressed as follows [42]–[43].

$$\Omega_b = \sqrt{\frac{V_{\alpha\beta\_\max}^{\;2}}{\frac{3}{2}(K_\Omega)^2 + (L_c \cdot p \cdot I_{\alpha\beta\_\max})^2}} \qquad (4)$$

Where K_Ω is motor constant, p is pole pairs, $I_{\alpha\beta\_max}$ is *rms* current value at maximum torque operating and $V_{\alpha\beta\_max}$ is the maximum inverter output voltage supplied to the PMSM. In a vehicular application, the DC link voltage is limited by the maximal battery voltage. Consequently, to extend the PMSM speed range, the SVPWM has to provide the largest possible magnitude [43].

The second objective is the power efficiency optimization. This has several aspects:

1.Minimize switching losses and ensure their equal-distribution between the 3H-bridges. The switching losses are an important part of the semiconductor power losses [44]. Reducing these losses is important to improve the inverter reliability because thermal stress is a key factor of the failure mechanism [19]. For the same reason, ensuring fair switching repartition is crucial.

2.Ability to feed the zero-sequence machine with the smallest voltage (V_0). In ideal PMSM, the back EMF e_0 component is null and consequently the average V_0 voltage has to be zero. But, even in this case, the set of four voltages may generate a zero-sequence voltage inducing zero-sequence current ripple (Δi_0). This current undulation has to be minimized to prevent pointless losses. This last point is crucial because the zero-sequence inductance value (L_0) is generally very small due to good phase magnetic coupling.

The third objective is the robustness of SVPWM control regarding:

1.The temporal accuracy of application times of the four chosen vectors. The control implementation is based on microcontroller and FPGA logic circuit using a digital timer. Timer precision as well as driver circuit and power switch delays introduce uncertainties in the real application. Moreover, internal dead time is mandatory to prevent leg short-circuit but it makes the actual PMSM voltage dependent on the current sign. This is another reason for the uncertainty on the voltage value actually applied.

2.The PMSM parameters. Any winding unbalance produces a non-null zero-sequence back EMF (e_0). In this real world context, the SVPWM sequence has to be able to generate a small non zero-sequence (V_0) with little harmonics content in order to counteract the PMSM defect.

In the following subsections, we use these specifications to analyze existing SVPWM techniques and provide innovative SVPWM strategies. Next subsection describes the two standard SVPWM methods.

D. Standard SVPWM Control Methods

Previous studies on SVPWM modulation techniques have already suggested two different strategies for a set of PMSM and 3-H bridge inverter.

The first method (Method I) discussed in [35] employs the 1st and 6th vector families. Fig. 4 - A shows the 3D representation of the selected voltages in the Concordia reference frame. Note that each selected vector develops a nonzero component in the zero-sequence subspace.

The second standard SVPWM strategy (Method II) utilizes the single vector of family V, the two vectors of family VI and the six vectors of family II [34]. Fig. 4 - B depicts the 3D representation of the discrete voltages defined by this method.

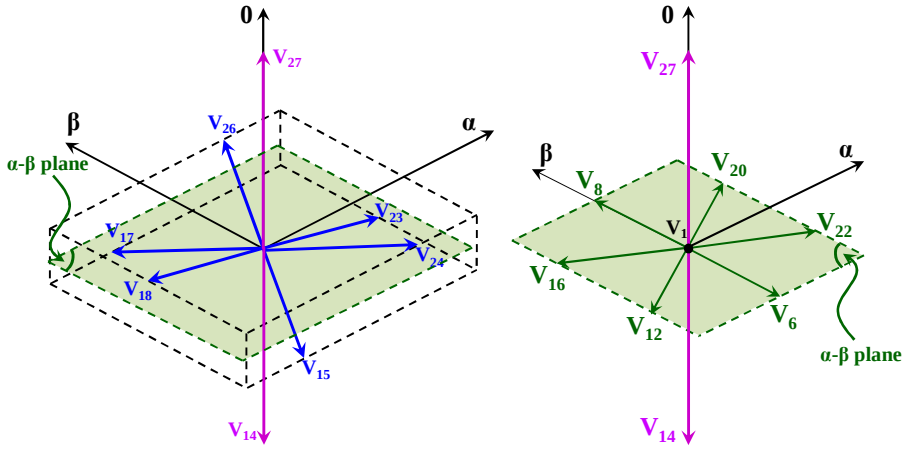

Fig. 4. Selected vectors of standard SVPWM modulation methods. (A) Method I, (B) Method II.

To date, 2 vector families have been neglected in the PWM generation. It is therefore interesting to explore other SVPWM strategies. The following sets out the proposed space vector control methods.

Both of the standard methods are restricted in the use of possibilities offered by the 3-H bridge inverter. Families III and IV are unused and each standard method is based on a unique main family (namely family I and family II for method I and method II respectively). It is interesting to explore other voltage combinations to solve (2) and to check their ability to respect the listed drive requirements. The following subsection sets out new space vector control methods.

E.Innovative SVPWM Control Methods

The diagram depicted in Fig. 5 shows the vector families used by the three proposed control technique. In Method III, family VI is voluntarily eliminated in order to reduce the instantaneous voltage of the zero-sequence fictitious machine. However, the maximum achievable voltage may be reduced since family III has small magnitude vectors. To tackle this problem, we propose Method IV which uses the largest voltages vectors (families I and II). To enable equation (3) resolution, Method IV uses also

family VI; these two vectors give the ability to reach the zero-sequence demand. Method V selects the smallest vectors (family III); the aim is to examine whether it leads to a relevant solution for small voltage requirement (generally corresponding to low motor speed). Note that family IV is rejected due to its high contribution in 0-axis.

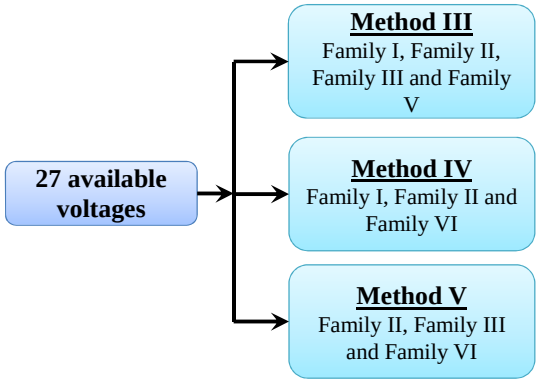

Fig. 5. Vectors set for the innovative proposed SVPWM strategies.

F. Comparative Study

Standard and suggested voltage vectors set have to be compared using the same criteria. Drive requirements impose the 3 mentioned constraints: speed range, power efficiency and sensitivity regarding parameter and control uncertainties. Table II shows the electric characteristics of the motor drive on which this comparative study is conducted.

TABLE II
ELECTRIC CHARACTERISTICS OF 3-HBRIDGE AND PMSM DRIVE

Symbol	Quantity	Value [a]
V_{dc}	DC link voltage	400 [V]
T	Switching period	100 [µs]
P_n	Rated power	40 [kW]
I_n	Rated *rms* current	66.67 [A]
K_Ω	Motor constant	0.70736 [V.s/rad]
p	Number of pole pairs	4
R	Phase winding resistance	75 [mΩ]
L_0	Leakage inductance	0.265258 [mH]
L_c	Cyclic inductance	2.652582 [mH]

1) *Mechanical Drive performance*: In ideal PMSM case, the reference voltage has a null zero-sequence component. Combining this constraint ($V_0^*=0$) with (3), the resulting voltages are given by:

$$\begin{bmatrix} V_\alpha^* \\ V_\beta^* \end{bmatrix} = \frac{1}{T_{sw}} \begin{bmatrix} V_{\alpha 1} & V_{\alpha 2} & V_{\alpha 3} & V_{\alpha 4} \\ V_{\beta 1} & V_{\beta 2} & V_{\beta 3} & V_{\beta 4} \end{bmatrix} \begin{bmatrix} \Delta t_1 \\ \Delta t_2 \\ \dfrac{(V_{04})(T_{sw}/2) + (V_{01} - V_{04})\Delta t_1 + (V_{02} - V_{04})\Delta t_2}{V_{04} - V_{03}} \\ T_{sw}/2 - \Delta t_1 - \Delta t_2 - \dfrac{(V_{04})(T_{sw}/2) + (V_{01} - V_{04})\Delta t_1 + (V_{02} - V_{04})\Delta t_2}{V_{04} - V_{03}} \end{bmatrix} \quad (5)$$

Varying the two remaining times Δt_1 and Δt_2 arbitrarily from 0 to $T_{sw}/2$ allows the exploration of all the possibilities. Referring to (4), each base speed corresponds to the highest voltage magnitude that the corresponding strategy can achieve on a complete electrical turn. Table III summarizes the computed results. Method III and Method IV have the best performance regarding this criterion. From table III, we can notice that the first four methods allow roughly the same speed range whereas, as expected, method V prevents high speeds.

TABLE III
ABILITY OF METHODS TO REACH HIGH SPEED

	Method I	Method II	Method III	Method IV	Method V
Base speed Ω_b	3116 rpm	3115 rpm	3128 rpm	3128 rpm	1626 rpm

By solving (3), a given reference voltage can lead to several combinations of four voltages set. But minimizing the torque ripple conducts to reduce the α-β current ripple (refer to (2)) and consequently α-β voltage ripple (refer to (1)). The scalar projection of methods vectors onto α-β plane defines sectors. As depicted in Fig. 6, there are six sectors for the standard methods and twelve for the proposed ones. From this representation, it is clear that the reduction of the voltage differences and therefore of the voltage ripple involves using adjacent vectors in a defined sector.

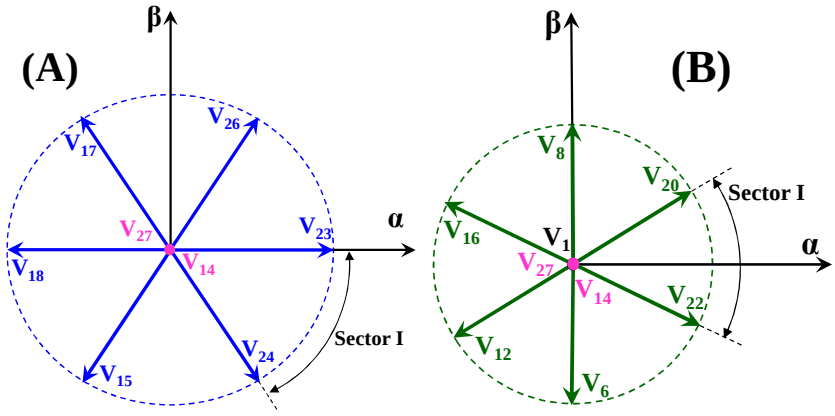

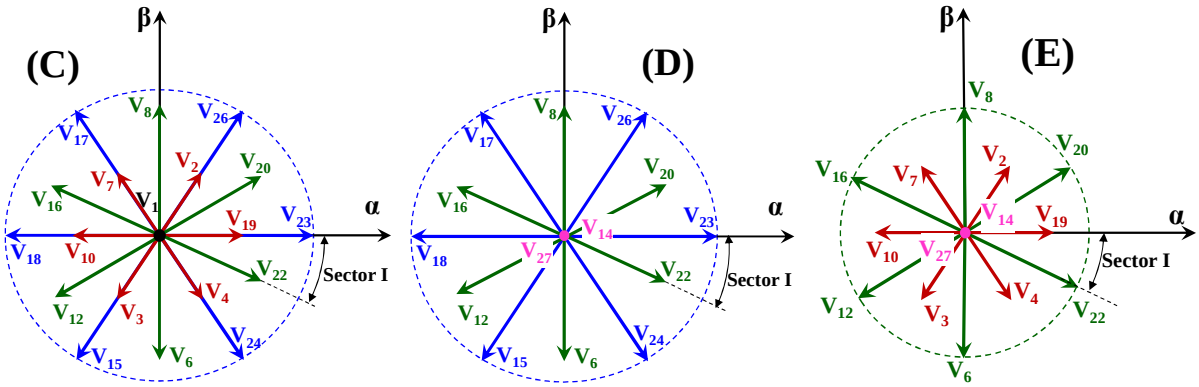

Fig. 6. Scalar projection of methods vectors onto α-β plane. Associated Sectors. (A) Method I, (B) Method II, (C) Method III, (D) Method IV, (E) Method V.

2) *Power efficiency optimization*: The reference vector is located in a unique sector associated to a single set of four voltages including, for some methods vector, V_{27} and V_{14} (Fig. 6). To minimize switching losses, it is crucial to construct a sequence guaranteeing an equitable distribution of the number of switches per leg, to obtain a limited number of switches and to avoid excessive switching while sector changing. Taking the first sector as an example, Fig. 7 illustrates the turn-on and turn-off numbers. The 3H-bridges are represented by three rectangles. Points inside them depict the number of switches achieved from the beginning of the half period: red points depict current switches while black ones symbolize previous switches. For instance, a single H-bridge needs two switches, 1 turn-on and 1 turn-off, to switch from the normalized voltage +1 to –1 or vice versa.

Finally every method gives the same number of switches (namely six) and ensures their equal distribution (2 per bridge) except Method II. This latter requires 7 switches which are necessarily asymmetrically distributed.

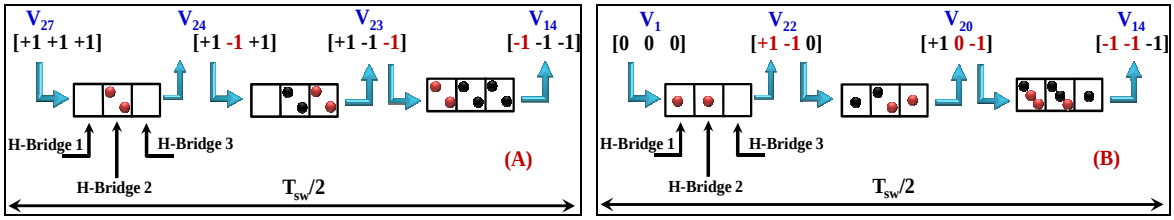

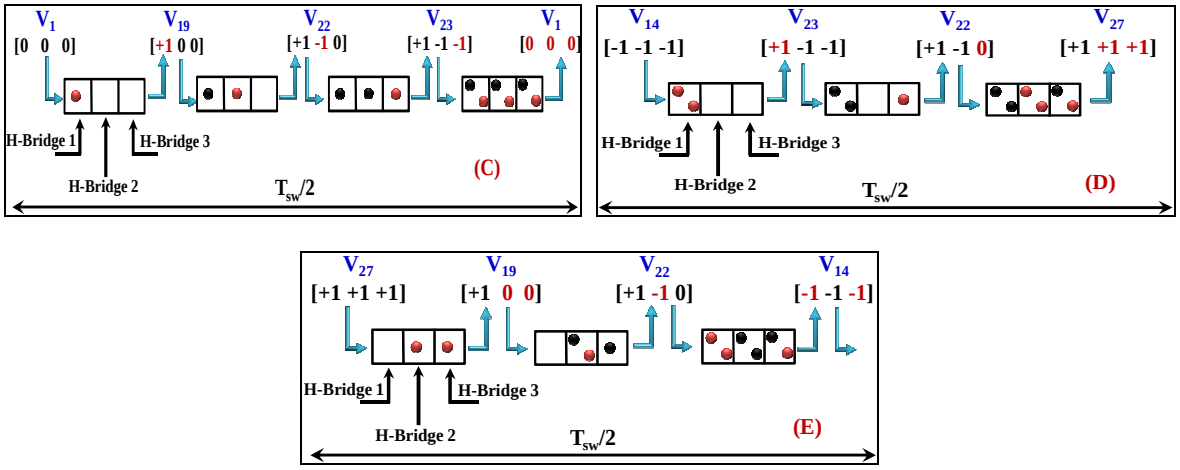

Fig. 7. Switching distribution in the 3H-bridges. (A) Method I, (B) Method II, (C) Method III, (D) Method IV, (E) Method V.

For each method, the selected sequence also involves a temporal evolution of the zero-sequence voltage component. This point is a crucial issue since it drives current ripple and related ohmic losses. For this purpose, (5) is used to determine any voltage with a null mean zero-sequence component. However, the instantaneous value of zero sequence voltage is not necessarily null, as shown in Fig. 8. The resulting current ripple is filtered by the zero-sequence impedance of the motor. As the switching period T_{sw} has a low value compared to electric motor time constant (L_0 / R), a fair approximation of this ripple Δi_0 (Fig. 8) is given by the $\delta i_0(t)$ peak to peak evaluation where $\delta i_0(t)$ is computed, on each switching period as:

$$\Delta i_0(t) = \frac{1}{L_0}\int_0^t V_0(\tau).d\tau \qquad (6)$$

The corresponding results are illustrated in Fig. 9. Clearly, the current ripple is highly dependent on the method used and on the voltage magnitude (and therefore on the motor speed) as seen in Fig. 9-A to Fig. 9-E. In low speed conditions, methods using family VI to achieve a null α-β voltage generate a important Δi_0. That is the reason why, with respect to this criterion, methods I, II, IV and V have poor performance at low speed. However, method III is particularly interesting. It makes use of null voltage vector V_1 to reduce the desired voltage magnitude; hence this method produces a very low Δi_0 at low speed.

Similarly, this ripple remains low at high speed because the two discrete voltage with non-null 0-component are applied consecutively and have the smallest 0-component (families I and III). Lastly, for the current ripple, it is not interesting to combine method V at low speed with any other method at high speed (Fig. 9-E).

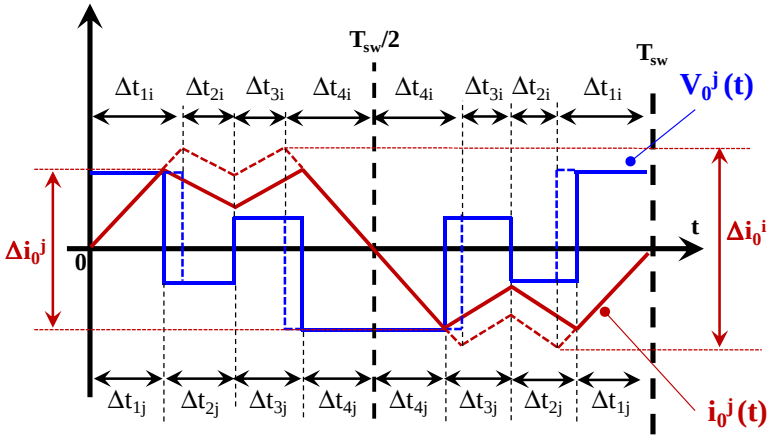

Fig. 8. Zero-sequence voltage and current waveforms in generic case.

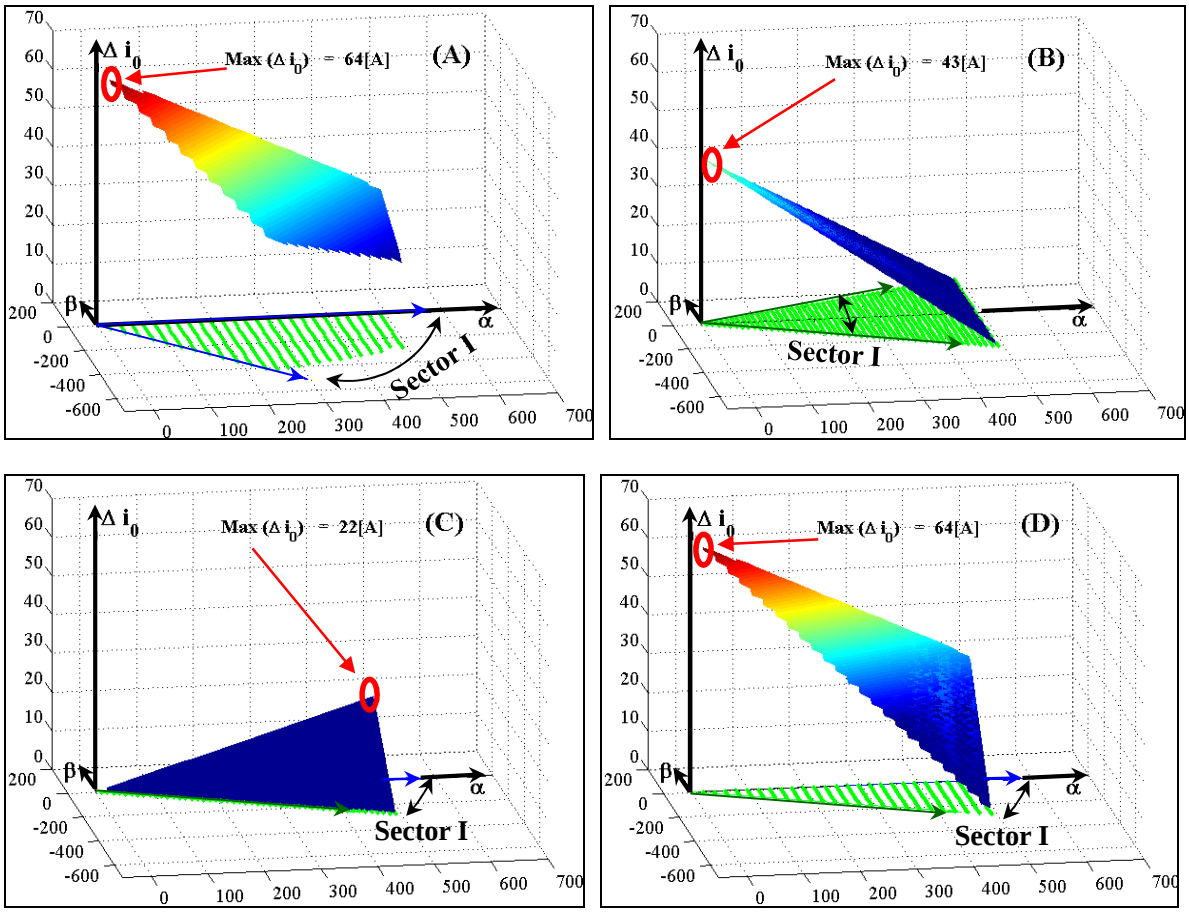

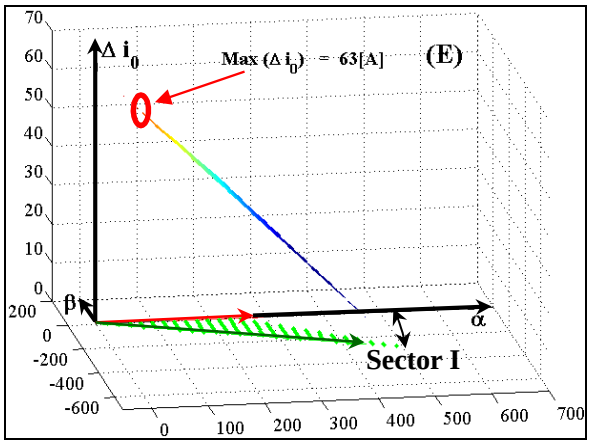

Fig. 9. Zero-sequence current ripple versus the average reference voltage. (A) Method I, (B) Method II, (C) Method III, (D) Method IV, (E) Method V.

3) *Robustness:* The first four methods are able to generate the same desired voltage amplitude while respecting $V_0^* = 0$. It is also essential to check the sensitivity of the computed duty cycles regarding implementation uncertainties. Motor control solutions are often based on numeric PWM implementations (with timers using a clock). For this reason, each time (Δt_k, $k = 1 \rightarrow 4$) is discretized and each related duty cycle is scalable in time steps of clock period. A typical value nowadays is 25ns. For this purpose, two tests are performed. The first one considers the motor-inverter behavior in the ideal case, while the second is the real case with unbalanced back EMF or imprecise duty cycles.

For the first case, (5) is solved using the same incremental step (namely $T_{sw}/50$) for Δt_1 and Δt_2. Fig. 10 shows the achievable voltage vectors for each method, represented by points in each studied sector. Points obtained with Method II and Method III are close together and consequently form a higher density than the three other methods. It reveals that Method II and Method III are less sensitive to duty cycle variations.

For the second case, (3) is solved using the same incremental step (namely $T_{sw}/25$) for every discrete voltage duration (Δt_k, $k = 1 \rightarrow 4$). The corresponding voltages are selected if the zero-sequence average voltage has a small value, namely $|V_0| \leq (V_{dc}/100)$.

Table IV summarizes the number of points obtained by the five methods for a given resolution (50 and 25 incremental steps) following the two tests. The first row indicates the results in ideal case, and the second one those obtained in the real case. Both results present the same trends.

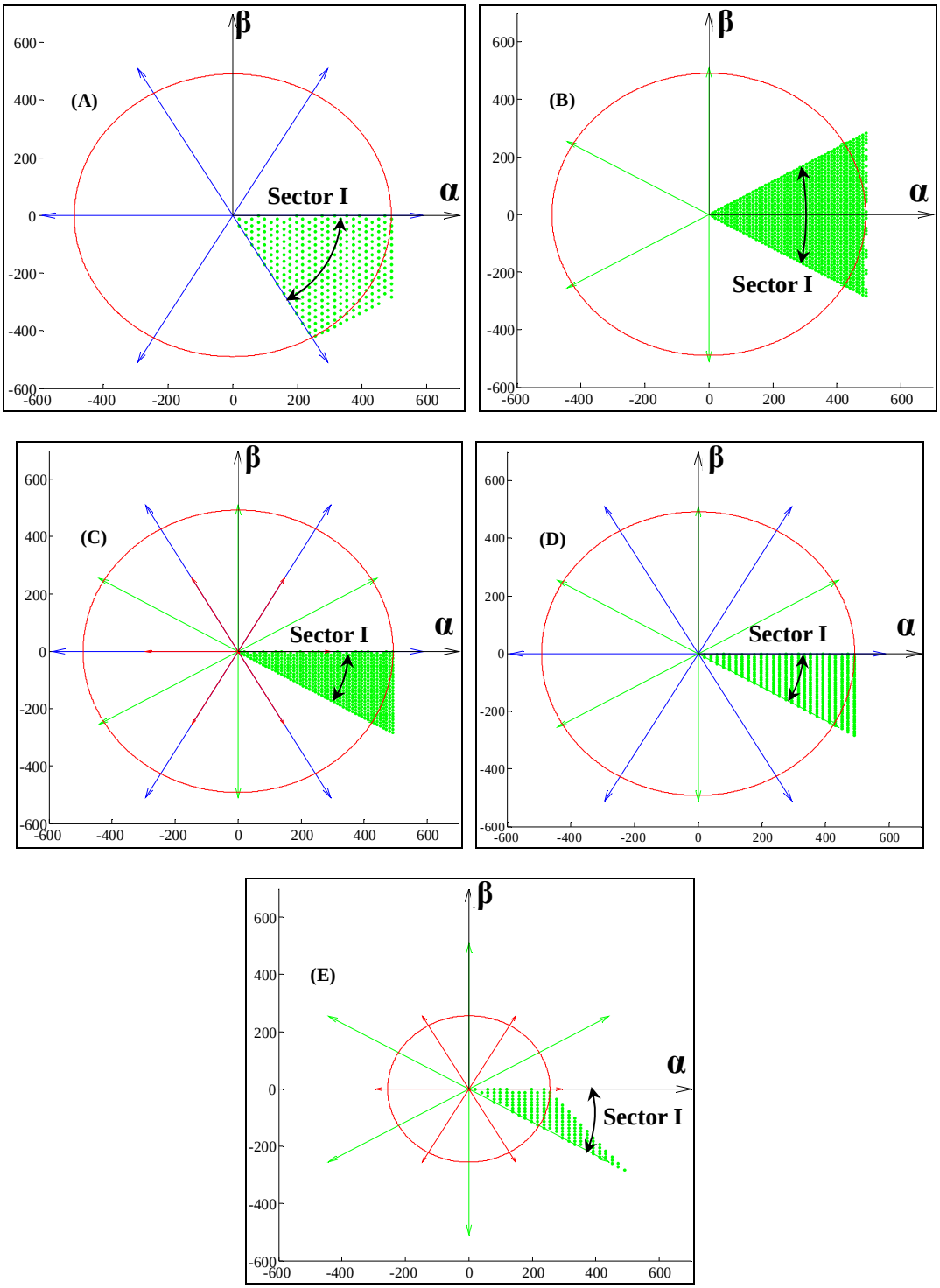

Fig. 10. Achievable reference voltages respecting $V_0 = 0$ constraint. . (A) Method I, (B) Method II, (C) Method III, (D) Method IV, (E) Method V.

TABLE IV
NUMBER OF ACHIEVABLE REFERENCE VECTORS

V_0 constraint	Method I	Method II	Method III	Method IV	Method V
$V_0 = 0$	*331*	*1305*	*1326*	*1002*	*332*
$\|V_0\| \leq (V_{dc}/100)$.	*453*	*2885*	*4142*	*1190*	*582*

Table V summarizes the whole comparative analysis. Advantages and drawbacks of each modulation technique are evaluated against each performance criterion. In conclusion, the innovative SVPWM Method III seems to be the best candidate for the electric drive control. It meets all the above-mentioned control drive specifications. To complete this comparison, the following subsection presents the SVPWM control implementation of this proposed method and a competing method, namely Method I.

TABLE V
SUMMARY OF COMPARATIVE STUDY

Criteria	Method I	Method II	Method III	Method IV	Method V
Ability to reach high base speed	+	+	+	+	−
Ability to generate null zero-sequence voltage	−	+	+	+	+
Switching losses minimization and equal-repartition	+	−	+	+	+
Ability to keep low zero-sequence current ripple	−	0	+	−	−
Insensitivity to duty-cycle variations	−	+	0	−	−

G. Space Vector PWM Implementation

In electric automobile applications, PM synchronous motors are driven using field-oriented control [41]. This technique is applied in synchronous rotating frame (0dq) in order to get DC quantities which can be regulated without steady-state error by simple PI correctors [45]. Fig. 11 shows the generic self-control diagram that is implemented in this study. The control loop purpose is to force the i_d and i_0 currents to zero and to meet the torque demand using only i_q current. This can be calculated using the following expression [46]:

$$i_q^* = \frac{1}{K_\Omega} \cdot T_{em}^* \qquad (7)$$

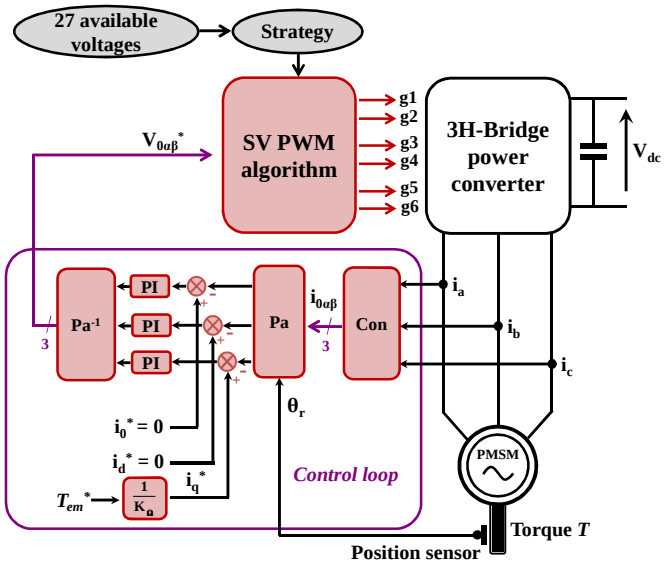

Fig. 11. Synoptic of proposed control architecture.

The control loop generates sinusoidal reference voltages $V_{0\alpha\beta}^*$ in the stationary 0αβ frame. The 3-H bridge inverter produces only 27 discrete voltages. The SVPWM algorithm blocks generate the required voltages using the technique of switching modulation. Fig. 12 shows SVPWM implementation diagram allowing the determination of the power switches gate signals. At a switching period T_{sw}, algorithm first locates the reference voltage $V_{0\alpha\beta}^*$ in the α-β frame and deduces the current sector and hence the four appropriate vectors. Second, it determines each duty cycle. Third, it defines the related switching sequence. Finally, the gate signals are generated with a small sampling time (i.e. $T_{sample} = T_{sw}/1024$).

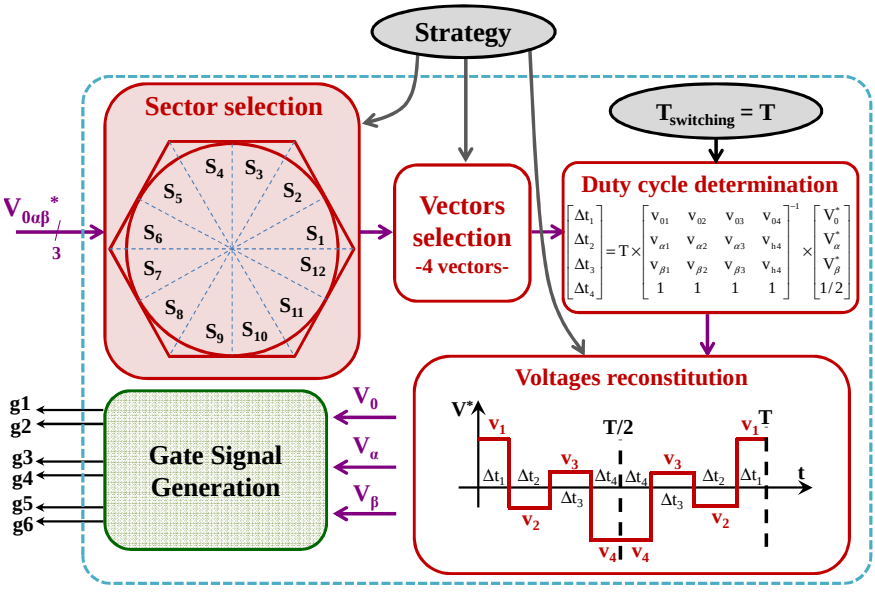

Fig. 12. Algorithm diagram of SVPWM modulation technique.

H. Results and Discussions

As shown in Fig. 11, the combination of PMSM and 3 H-bridge inverter associated with its dedicated control scheme have been tested in simulation using Matlab/Simulink software tools. The DC link voltage is kept constant along the operation. The PMSM model does not include a mechanical model. Only steady operation at a fixed speed (specifically 955 rpm) and with a constant reference torque (namely 60 N.m) are examined. Fig. 13 shows the results obtained with two control methods (i.e. I and III). Furthermore it should be noted that all methods have the same complexity since they are based on solving equation (3).

Fig. 13-A and Fig. 13-B show instantaneous electromagnetic torque obtained for a SVPWM switching frequency forced to (f_{sw}) = 1/T_{sw} =10 kHz. In each case, the motor produces accurately the requested torque, proving the correct operation of the implemented self-control algorithm. The torque ripple is almost insensitive to the SVPWM method. At a constant speed N = 955 rpm, the zero-sequence currents and the three stator currents (i_a, i_b, i_c) are respectively plotted in [Fig. 13-C - Fig. 13-D] and [Fig. 13-E - Fig. 13-F]. Simulation results confirm the conclusions of the comparative study. Method III has an advantage over others in providing a low zero-sequence current ripple Δi_0. For instance, this operating point (N = 955 rpm; T_{em} = 60 N.m) reveals (Δi_0) = ±6A when using Method III but ± 56.2A with Method I. Hence method III is favourable both in terms of power efficiency and electromagnetic compatibility. In addition, Fig. 14 verifies that method I increases Δi_0 at low speed (low voltage) contrary to method III which tends to reduce it.

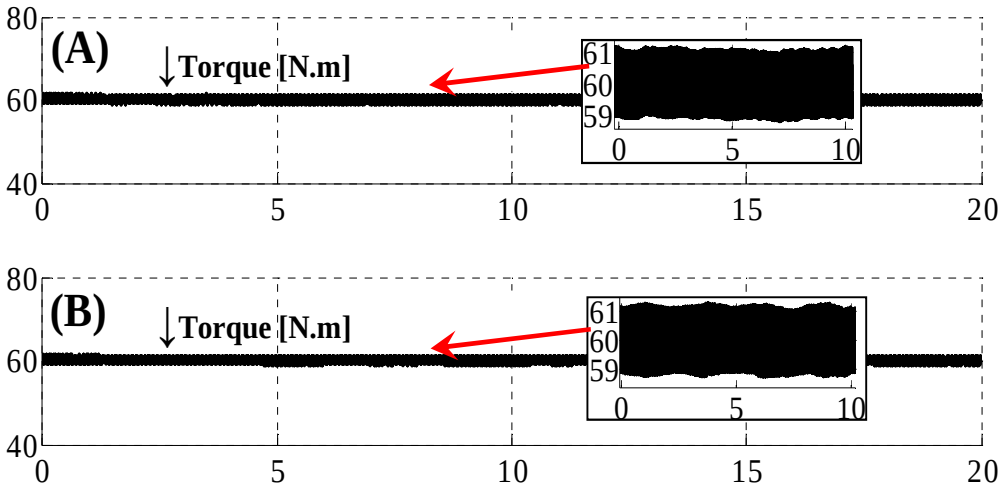

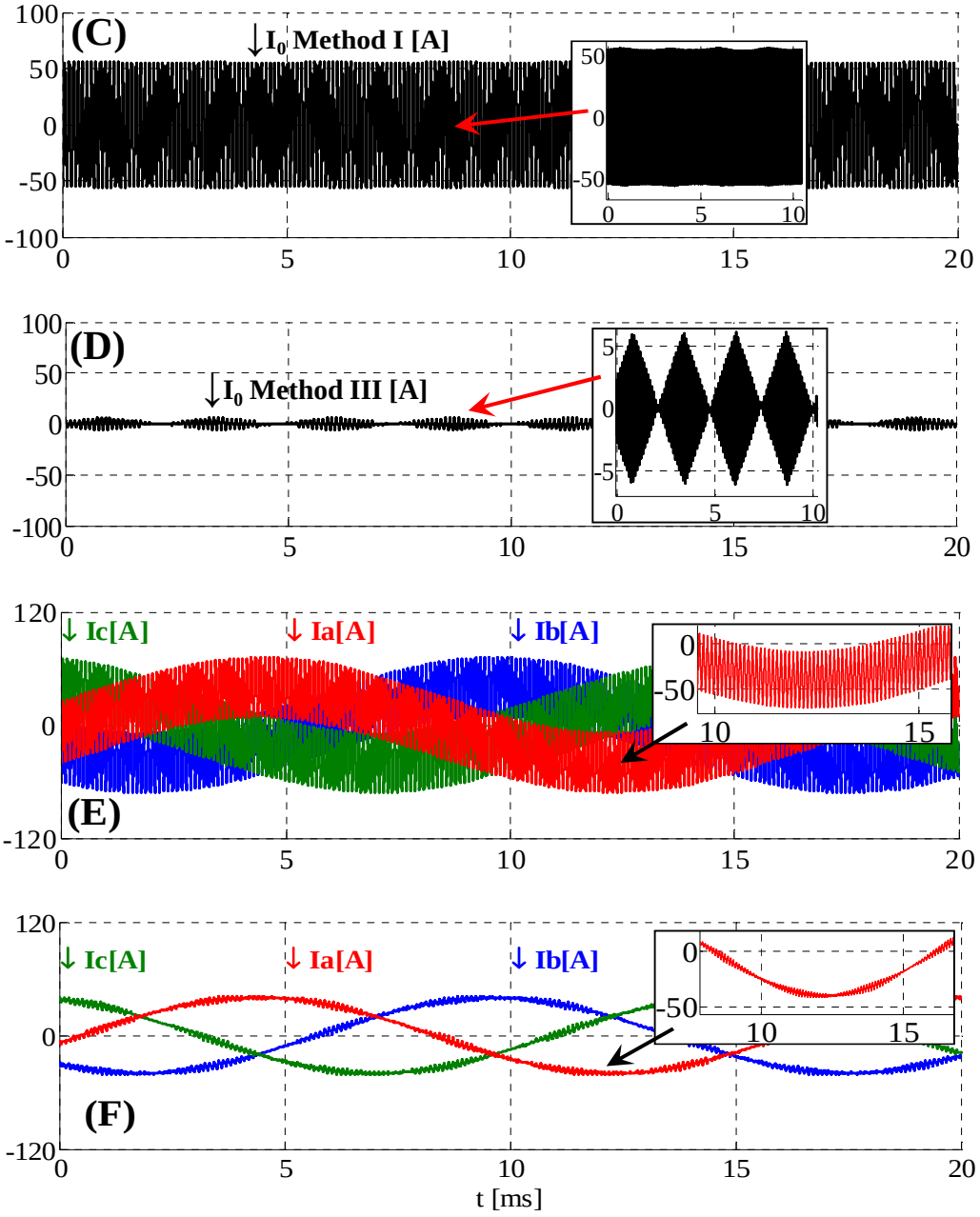
(C)
↓I0 Method I [A]
(D)
↓I0 Method III [A]
↓ Ic[A]
↓ Ia[A]
↓ Ib[A]
(E)
(F)
t [ms]

Fig. 13. SVPWM methods comparison in self-control mode.

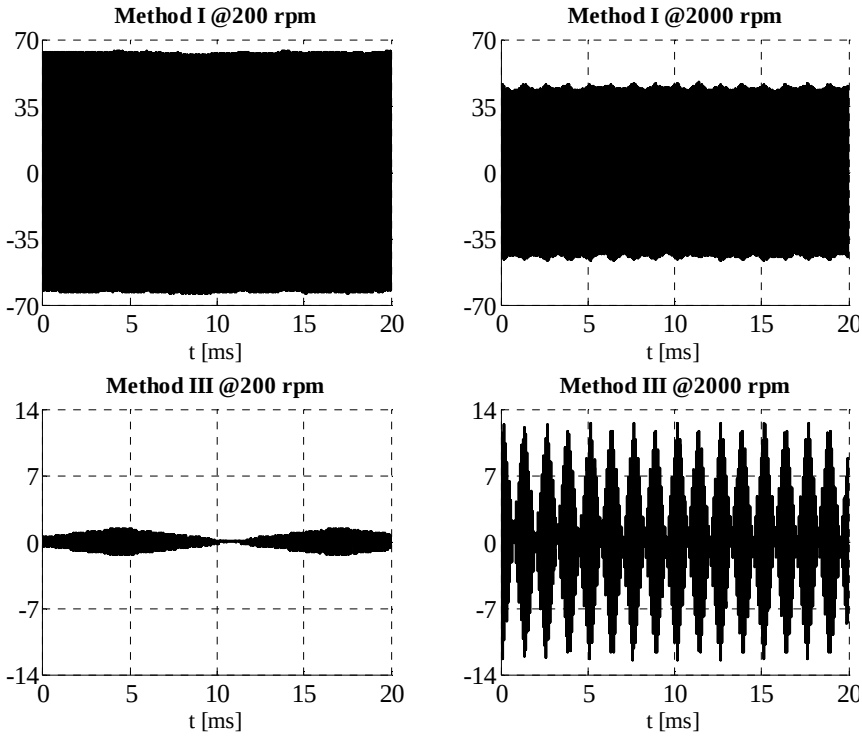

Fig. 14. Zero-sequence current at T_{em}=60 N.m (200 rpm / 2000 rpm).

For Control design, the combination of a PMSM and a 3-H bridge inverter offer important degrees of freedom. The SVPWM synthesis reveals a significant number of strategies. This exhaustive study was based on a comprehensive inventory of the EV drive requirements. The quantitative analysis allows the identification of a new and more attractive option. Simulation results confirm the interest of this choice.

The drive architecture was analyzed in nominal mode. The second crucial issue is to explore its abilities to operate in degraded mode. The following section gives an overview of the degraded mode possibilities and proposes fault-tolerant control where feasible.

IV. Exhaustive Analysis Of Failure Mode

The studied system may encounter fault conditions. As mentioned in section II, power switches have the largest failures occurrence and their occurrence has very significant implications. Switch breakdown may result in switch open circuit (OC) or switch short-circuit (SC). In practice, the SC switch failure is most common compared to the OC failure (85% for SC and 15% for OC) [47]. For that reason, section V:

1) explains drive remaining possibilities once a single power switch becomes inoperative,

2) suggests fault tolerant mode control algorithm.

For simplicity, a semiconductor breakdown (precisely (T_2, D_2)) of the third bridge (i.e. phase *C*) is considered.

Remaining Discrete Space Vectors: Fig. 15 represents switch states during a short - circuit failure on a single power switch (T_2, D_2). In this case, the common gate driver leg forces power switch (T_3, D_3) to be immediately in open state.

When such a fault occurs, the affected H-bridge can only produce two different levels instead of three, namely 0 and $+V_{dc}$ (example in Fig. 15). As a result, the inverter is only able to produce eighteen discrete space vectors, that is to say half the normal case. These cases are listed in Table VI while Fig. 16 illustrates them in Concordia reference frame.

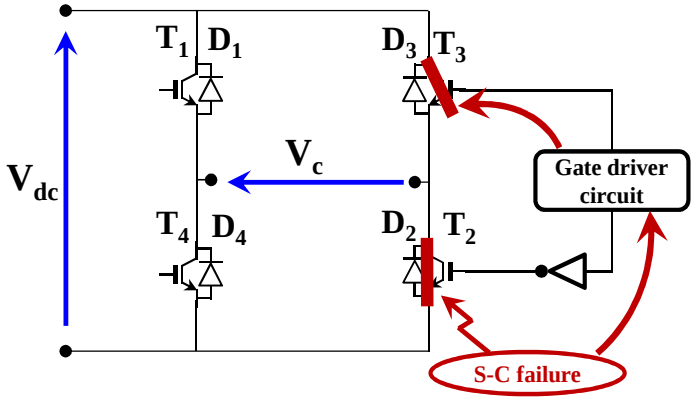

Fig. 15. Short-circuit (SC) switch failure case.

TABLE VI
STATOR VOLTAGES DECOMPOSITION

VECTORS	V_a	V_b	V_c	V_0	V_α	V_β
V_1	0	0	0	0	0	0
V_3	0	0	+1	$\sqrt{3}/3$	$-\sqrt{1/6}$	$-\sqrt{2}/2$
V_4	0	–1	0	$-\sqrt{3}/3$	$\sqrt{1/6}$	$-\sqrt{2}/2$
V_6	0	–1	+1	0	0	$-\sqrt{2}$
V_7	0	+1	0	$\sqrt{3}/3$	$-\sqrt{1/6}$	$\sqrt{2}/2$
V_9	0	+1	+1	$2\cdot(\sqrt{3}/3)$	$-2\cdot\sqrt{1/6}$	0
V_{10}	–1	0	0	$-\sqrt{3}/3$	$-2\cdot\sqrt{1/6}$	0
V_{12}	–1	0	+1	0	$-\sqrt{3/2}$	$-\sqrt{2}/2$
V_{13}	–1	–1	0	$-2\cdot(\sqrt{3}/3)$	$-\sqrt{1/6}$	$-\sqrt{2}/2$

V_{15}	–1	–1	+1	$-\sqrt{3}/3$	$-2\cdot\sqrt{1/6}$	$-\sqrt{2}$
V_{16}	–1	+1	0	0	$-\sqrt{3/2}$	$\sqrt{2}/2$
V_{18}	–1	+1	+1	$\sqrt{3}/3$	$-4\cdot\sqrt{1/6}$	0
V_{19}	+1	0	0	$\sqrt{3}/3$	$2\cdot\sqrt{1/6}$	0
V_{21}	+1	0	+1	$2\cdot(\sqrt{3}/3)$	$\sqrt{1/6}$	$-\sqrt{2}/2$
V_{22}	+1	–1	0	0	$\sqrt{3/2}$	$-\sqrt{2}/2$
V_{24}	+1	–1	+1	$\sqrt{3}/3$	$2\cdot\sqrt{1/6}$	$-\sqrt{2}$
V_{25}	+1	+1	0	$2\cdot(\sqrt{3}/3)$	$\sqrt{1/6}$	$\sqrt{2}/2$
V_{27}	+1	+1	+1	$\sqrt{3}$	0	0

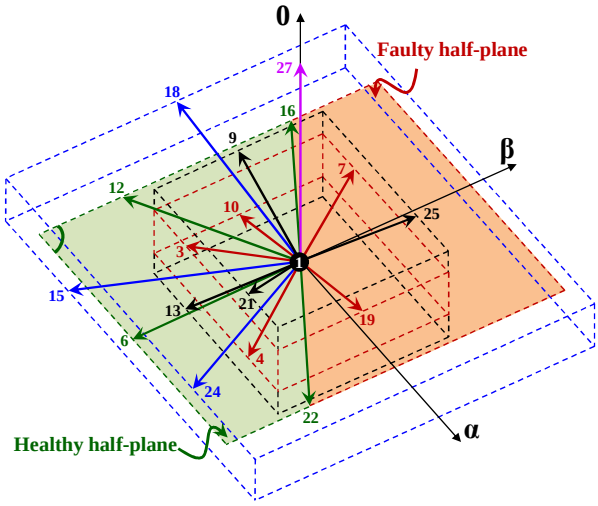

Fig. 16. Discrete SV in case of a single power switch in S-C.

Using a combination of family III and family IV space vectors, as suggested by the chosen SVPWM method, a rotating voltage can only be obtained in a half-plane delimited by V_{16} and V_{22}. Conversely, all discrete vectors of the opposite half plane reveals the same sign zero sequence component (positive in the present case).

Exhaustive Research of a Remedial Strategy: In faulty drive, the first objective is to obtain a rotating voltage in the α-β frame by using combinations of the remaining discrete voltages. The second objective is to realize a voltage with a null mean zero-sequence component during a switching period ($<V_0> = 0$). The zero sequence current i_0 is essentially limited by the zero sequence inductance whose value is low. Hence, as the three voltage components (V_α, V_β, V_0) still need to be controlled, the faulty PWM generation remains a 4-dimensional problem. Any achievable voltage is determined by using (5) while varying Δt_1 and Δt_2 arbitrarily from 0 to $T_{sw}/2$. In this equation, {*V1*, *V2*, *V3*, *V4*} is a set of four

selected voltages out of the remaining eighteen ones. Consequently, the number of possible combinations is 3060 (C_{18}^{4} = 3060). A given voltage can be achieved by different voltage sets. On the contrary, some voltages may never be realized. Obviously, solving (5) is constrained by positive times Δt_3 and Δt_4.

Fig. 17-A shows the SV reachable area defined in case of a single power switch SC. It is a half hexagon; the missing part is due to inability to meet the $V_0 = 0$ specification. Consequently, it shows that a rotating voltage cannot be obtained using the remaining discrete vectors.

As given in Table VI, the high zero-sequence component of vector V_{25} ($2\cdot(\sqrt{3})/3$) prevents null V_0 in the critical region. Among the 18 remaining vectors, the only ones which permit to reduce this high voltage are V_4, V_{10} and V_{13}. V_{13} is the opposite of V_{25} (see Fig. 17-A) and the zero-sequence component of the two vectors V_4 and V_{10} are half of V_{25} one. The diagram depicted in Fig. 17-B illustrates a typical SVPWM combination containing V_4 and V_{25}. It shows that for a given duty cycle (σ) of V_{25}, double this value (2σ) must be applied to V_4 in order to generate a null V_0. Consequently, the scalar projection of the resulting reference voltage is always located in the healthy region.

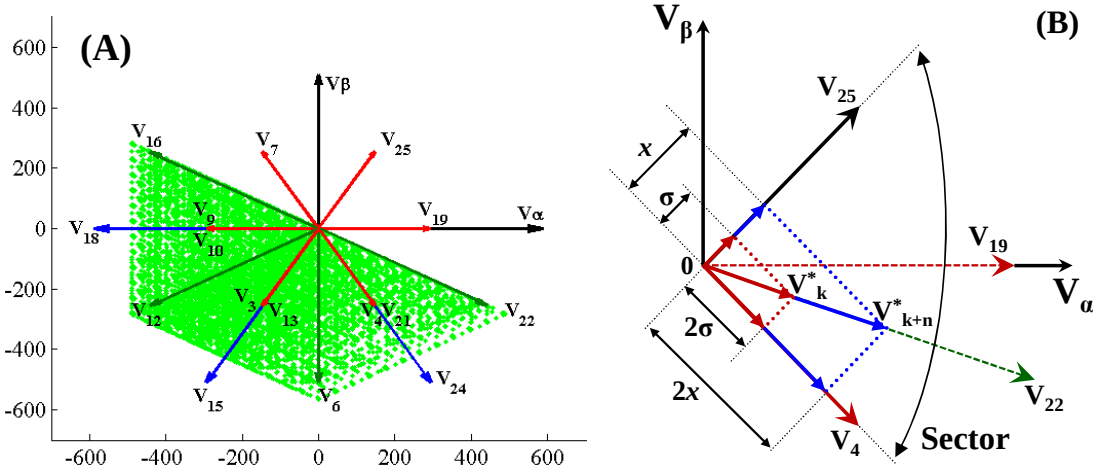

Fig. 17. Achievable reference voltages in case of single power switch in short-circuit states.

To summarize, a satisfactory behavior in degraded operating mode can't be obtained without a reconfiguration of the power converter structure. Indeed, considering a phase disconnection of the faulty H-bridge, it could lead to a more suitable degraded operating mode. This topic will be studied in a future work and presented in a forthcoming paper.

V. CONCLUSION

This paper has considered H-Bridge power converter for a three-phase PM synchronous motor in an electric vehicle (EV).

Firstly, using a methodical approach, innovative space vector PWM (SVPWM) control methods has been proposed. Furthermore, using the EV drive requirements, these suggested methods has been compared to standard SVPWM ones. Among these, a specific one has combined all the advantages: minimization of switching losses, balancing of switching rate between the three H-bridges, insensitivity to duty-cycle, maximization of the drive performance, and reduction of the zero-sequence current ripple. This proposed method has been successfully implemented in simulation with a self-controlled PM motor model using Matlab-Simulink® environment.

Secondly, power switch failure mode has been fully investigated. Exhaustive analysis of the most common breakdown demonstrates that short-circuit (SC) is critical state regarding the margins left in the control strategy. Future works will be focused on the SVPWM control methods in normal and degraded operating modes.

Finally, it has been demonstrated that no satisfactory post-failure reconfiguration can be applied if the disconnection of the PMSM phase from the failing H-bridge is not considered. The work presented in this paper has been a first step in defining fault tolerant control for an EV power train.

ACKNOWLEDGEMENT

Authors would like to thank the French ministry of Industry, in the context of the project SOFRACI "*Structure d'Onduleur Fort Rendement A fonction Charge Intégrée*", 2009 to 2012, for its financial support to this research work.

VI. REFERENCES

[1] M. Ciappa, "prediction on the base of mission profiles," *Microelectronics Reliability*, vol. 45, no. 9–11, pp. 1293–1298, Sep. 2005.

[2] V. Smet, F. Forest, J. Huselstein, F. Richardeau, Z. Khatir, S. Lefebvre, and M. Berkani, "Ageing and Failure Modes of IGBT Modules in High-Temperature Power Cycling," *IEEE Trans. Ind. Electron.*, vol. 58, no. 10, pp. 4931–4941, Oct. 2011.

[3] D. Martineau, T. Mazeaud, M. Legros, Ph. Dupuy, and C. Levade, "Characterization of Alterations on Power MOSFET Devices under Extreme Electro-thermal Fatigue," *Microelectronics Reliability*, vol. 50, no. 9-11, pp. 1768–1772, Sep. 2010.

[4] N. Bianchi, S. Bolognani, M. Zigliotto, and M. Zordan, “Innovative Remedial Strategies for Inverter Faults in IPM Synchronous Motor Drives,” *IEEE Trans. Energy Convers.*, vol. 18, no. 2, pp. 306–314, Jun. 2003.

[5] J. Dixon, J. Pereda, C. Castillo, and S. Bosch, “Asymmetrical Multilevel Inverter for Traction Drives Using Only One DC Supply,” *IEEE Trans. Veh. Technol.*, vol.59, no.8, pp. 3736–3743, Oct. 2010.

[6] R. Wang, and J. Wang, “Fault-Tolerant Control with Active Fault Diagnosis for Four-Wheel Independently Driven Electric Ground Vehicles,” *IEEE Trans. Veh. Technol.*, vol.60, no.9, pp.4276–4287, Nov. 2011.

[7] D. Diallo, M.E.H. Benbouzid, and A. Makouf, “A fault tolerant control architecture for Induction Motor Drives in Automotive Applications,” *IEEE Trans. Veh. Technol.*, vol.53, no.6, pp. 1847–1855, Nov. 2004.

[8] M.E.H. Benbouzid, D. Diallo, and M. Zeraoulia, “Advanced Fault-Tolerant Control of Induction-Motor Drives for EV/HEV Traction Applications: From Conventional to Modern and Intelligent Control Techniques,” *IEEE Trans. Veh. Technol.*, vol.56, no.2, pp. 519–528, Mar. 2007.

[9] N. Bianchi, M.D. Pre, and S. Bolognani, “Design Of a Fault-Tolerant IPM Motor for Electric Power Steering,” *IEEE Trans. Veh. Technol.*, vol.55, no.4, pp. 1102–1111, Jul. 2006.

[10] L. De Sousa and B. Bouchez, “Combined Electric Device For Powering and Charging,” Patent WO 2010/057892 A1, 2010.

[11] L. De-Sousa, B. Bouchez, “Method and electric combined device for powering and charging with compensation means”, International Patent WO 2010/057893 A1, May 2010.

[12] L. De Sousa, B. Silvestre, and B. Bouchez, “A Combined Multiphase Electric Drive and Fast Battery Charger for Electric Vehicles Topology and Electric Propulsion Efficency Analysis,” in *Conf. Rec. IEEE VPPC Conf.*, France, 1–3 Sept. 2010, pp. 1–6.

[13] S. Lacroix, M. Hilairet, and E. Laboure, “Design of a Battery-Charger Controller for Electric Vehicle Based on RST Controller,” in *Conf. Rec. IEEE VPPC Conf.*, USA, 6–9 Sep 2011, pp. 1–6.

[14] H. Schwab, A. Klönne, S. Reck, I. Ramesohl, G. Sturtzer, and B. Keith, “Reliability Evaluation of a Permanent Magnet Synchronous Motor Drive for an Automotive Application,” in *Conf. Rec. IEEE EPE 10th Euro. Conf.*, 2–4 Dec 2003, pp. 1–10.

[15] L. Dulau, S. Pontarollo, A. Boimond, J.-François Garnier, N. Giraudo, and O. Terrasse, “A New Gate Driver Integrated Circuit for IGBT Devices with Advanced Protections,” *IEEE Trans. Power Electron.*, vol. 21, no. 1, pp. 38–44, Jan. 2006.

[16] M. Bouarroudj-Berkani and L. Dupont, “ Fatigue des composants électroniques de puissance-Physique de défaillance,” *Techniques de l'Ingénieur*, vol. 3126, pp. 1–21, 2010 (text in French).

[17] M. Bouarroudj, Z. Khatir, J. P. Ousten, L. Dupont, S. Lefebvre, and F. Badel, “Comparison of Stress Distributions and Failure Modes During Thermal Cycling and Power Cycling on high Power IGBT Modules,” in *Conf. Rec. IEEE APE Euro. Conf.*, Denmark, 2–5 Sept. 2007, pp. 1 –10.

[18] G. Coquery, G. Lefranc, T. Licht, R. Lallemand, N. Seliger, and H. Berg, “High Temperature Reliability on Automotive Power Modules Verified by Power Cycling Tests up to 150°C,” *Microelectronics Reliability*, vol. 43, no. 9–11, pp. 1871–1876, Sep. 2003.

[19] G. Coquery, S. Carubelli, J.P. Ousten, R. Lallemand, F. Lecoq, D. Lhotellier, V. de Viry and Ph. Dupuy, “Power module lifetime estimation from chip temperature direct measurement in an automotive traction inverter,” *Microelectronics Reliability*, vol. 41, no. 9-10, pp. 1695–1700, Sep. 2001.

[20] M. Ciappa, “Selected Failure Mechanisms of Modern Power Modules,” *Microelectron. Reliab.*, vol. 42, no. 4/5, pp. 653–667, Apr./May 2002.

[21] J. Vallon, F. Richardeau, H. Feral, Y. Cheron, F. Forest, J.-J. Huselstein and C. Joubert, “Converter Topology for Reliability Test Bench Dedicated to PWM Inverters,” in *Conf. Rec. Power Electronics and Applications*, France, 2003, pp. 1–10.

[22] F. Richardeau, Ph. Baudesson, and T.A. Meynard, “Failures-tolerance and remedial strategies of a PWM multicell inverter,” *IEEE Trans. Power Electron.*, vol. 17, no. 6, pp. 905–912, Nov. 2002.

[23] S. Lefebvre, Z. Khatir, and F. Saint-Eve, “Experimental Behavior of Single-Chip IGBT and COOLMOS Devices Under Repetitive Short-Circuit Conditions,” *IEEE Trans. Electron Devices*, vol. 52, no. 2, pp. 276–283, Feb. 2005.

[24] F. Richardeau, J. Mavier, H. Piquet, and G. Gateau, “Fault-Tolerant Inverter for on-Board Aircraft EHA,” in *Conf. Rec. IEEE EPE 12th Euro. Conf.*, Denmark, 2–5 Sep 2007, pp. 1–9.

[25] B.A. Welchko, T.A. Lipo, T.M. Jahns, and S.E. Schulz, "Fault tolerant three-phase AC motor drive topologies: a comparison of features, cost, and limitations," *IEEE Trans. Power Electron.*, vol.19, no.4, pp. 1108–1116, Jul. 2004.

[26] J. Mecrow, B.C. Jack, A.G. Haylock and J.A. Coles, “Fault-Tolerant Permanent Magnet Machine Drives,” in *IEE Proc. Electr. Power Appl.*, vol. 143, no. 6, pp. 437 –442, 1996.

[27] L. De Sousa and H. Dogan, “Method of Evaluating the Zero-Sequence Inductance Ratio for Electrical Machines,” in *Proc. IEEE EPE 14th Euro. Conf.*, United Kingdom, 30 Aug.–1 Sept. 2011, pp. 1–10.

[28] B. Venugopal Reddy, V.T. Somasekhar, and Y. Kalyan, “Decoupled Space-Vector PWM Strategies for a Four-Level Asymmetrical Open-End Winding Induction Motor Drive with Waveform Symmetries,” *IEEE Trans. Ind. Electron.*, vol. 58, no.11, pp. 5130–5141, Nov. 2011.

[29] K.A. Corzine, S.D. Sudhoff, and C.A. Whitcomb, "Performance characteristics of a cascaded two-level converter," *IEEE Trans. Energy Convers.*, vol.14, no.3, pp.433–439, Sep. 1999.

[30] M-A. Shamsi-Nejad, B. Nahid-Mobarakeh, S. Pierfederici, and F. Meibody-Tabar, “Fault Tolerant and Minimum Loss Control of Double-Star Synchronous Machines Under Open Phase Conditions,” *IEEE Trans. Ind. Electron.*, vol. 55, no. 5, pp. 1956–1965, May. 2008.

[31] N. Ertugrul, W. Soong, G. Dostal, and D. Saxon, "Fault tolerant motor drive system with redundancy for critical applications," in *Conf. Rec. IEEE PElSC 33rd Annu. Conf.*, Australia, 23–27 June 2002, pp. 1457–1462.

[32] I.Y. Önel and M. E. H. Benbouzid, “Induction Motor Bearing Failure Detection and Diagnosis: Park and Concordia Transform Approaches Comparative Study,” *IEEE/ASME Trans. Mechatron.*, vol. 13, no. 2, pp. 257–262, Apr. 2008.

[33] F. Scuiller, J.-Frederic Charpentier, E. Semail, and S. Clenet, “Comparison of two 5-phase Permanent Magnet Machine Winding Configurations. Application on Naval Propulsion Specifications,” in *Conf. Rec. IEEE IEMDC*, Turkey, 3–5 May 2007 pp. 34–39.

[34] J. P. Martin, E. Semail, S. Pierfederici, A. Bouscayrol, and B. Davat, “Space Vector Control of 5-phase PMSM Supplied by 5 H-bridge VSIs,” *in Congrès International Electrimacs, Montréal*, 2002, pp. 1-6.

[35] X. Kestelyn, E. Semail, and J. P. Hautier, “Multi-phase System Supplied by SVM VSI : A New Fast Algorithm to Compute Duty Cycles,” *EPE Journal*, vol. 14, no. 3, pp. 1–11, 2004.

[38] R. Krishnan, *Permanent Magnet Synchronous and Brushless DC Motor Drives*, CRC Press, p. 611, Sep. 2009.

[37] J. P. Martin, “Contribution to the Voltage Supply of Multi-Phase Synchronous Permanent Magnet Machines: Normal and Fault Operating Modes,” Ph.D. thesis, Institut National Polytechnique de Lorraine Nancy, France, 2003 (text in French).

[38] T. Chen, “Circulating zero-sequence current control of parallel three-phase inverters,” in *IEE Proc. Electr. Power Appl.*, vol. 153, no. 2, pp. 282–288, 2006.

[39] Yifan Zhao , T. A. Lipo, “Space Vector PWM Control of Dual Three-phase Induction Machine using Vector Space Decomposition,” *IEEE Trans. on Ind. Applicat.*, vol. 31, no. 5, pp. 1100–1109, 1995.

[40] M. Zeraoulia, M.E.H. Benbouzid, and D. Diallo, “Electric Motor Drive Selection Issues for HEV Propulsion Systems: A Comparative Study,” *IEEE Trans. Veh. Technol.*, vol. 55, no. 6, pp. 1756–1764, Nov. 2006.

[41] I. Hussein, *Electric and Hybrid Vehicles; Design and Fundamentals*, 2nd ed., Boca Raton: CRC Press, p. 288, 2010.

[42] M. Stulrajter, V. Hrabovcoà, and M. Franko, “Permanent Magnet Synchronous Motor Control Theory,” *Journal of Electrical Engineering*, vol. 58, no. 2, pp. 79–84, 2007.

[43] J. M. Miller, *Propulsion Systems for Hybrid Vehicles, 2nd ed*, IET, The Institution of Engineering and Technology, Stevenage, UK, p. 593, Jan. 2010.

[44] Y. Xiong, S. Sun, H. Jia, P. Shea, and Z. J. Shen, “New Physical Insights on Power MOSFET Switching Losses,” *IEEE Trans. Power Electron.*, vol. 24, no. 2, pp. 525–531, Feb. 2009.

[45] Nahome Alemayehu A., R. Zaimeddine, Bing Liu and Tore Undeland, “Vector control of direct drive six phase permanent magnet synchronous generators,” *in Conf. Rec. IEEE PES PowerTech*, Trondheim, 19–23 June 2011, pp. 1–7.

[46] E. Semail, A. Bouscayrol, and J. P. Hautier, “Vectorial Formalism for analysis and design of polyphase synchronous machines,” *Eur. Phys. J.-Appl. Phys. (EPJAP)*, vol. 22, no. 3, pp. 207–220, 2003.

[47] J-P. Louis, Control of Non-conventional Synchronous Motors, Paris: Wiley, p. 448, 2011.